Output-Controllable Partial Inverse Digital Predistortion for RF Power Amplifiers

Chao Yu, *Student Member*, *IEEE*, Michel Allegue-Martínez, Yan Guo, *Student Member*, *IEEE*, and Anding Zhu, *Senior Member*, *IEEE*

***Abstract*—In this paper, an output-controllable digital predistortion (DPD) technique is proposed to partially inverse the nonlinear behavior of RF power amplifiers (PAs). Compared to the existing DPD, the proposed method changes the goal that the PA output must be exactly the same as the original input to a new one that the PA output can be arbitrarily controlled according to user's demand. The proposed approach largely expands the capability of digital predistortion and thus provides more flexibility for system designers to effectively use DPD to manipulate the PA output in order to handle more application scenarios and objectively conduct further system optimization. Various application cases have been tested. The experimental results demonstrate that the proposed approach has great potential in future wireless communication system design.**

***Index Terms*—Digital predistortion, linearization, multi-band, output control, power amplifiers, wideband**

I. Introduction

DUE to continuous reduction of cost and power consumption of digital circuits, more and more digital technologies have been involved in the conventional analog circuit design in order to improve system performance and conduct complex functions, which is called digitally assisted analog design. Digital predistortion (DPD), which utilizes digital techniques to compensate for nonlinear distortion induced by radio frequency (RF) power amplifiers (PAs), is one of the well-known digitally assisted analog design examples. With DPD, the PA can be operated at higher drive levels for higher efficiency without losing linearity. Many DPD models have been developed in the past decades, and DPD is widely employed in modern wireless communication systems [1]-[5] today. In single band transmitters, memory polynomial (MP) model [1], generalized memory polynomial (GMP) model [3], dynamic deviation reduction (DDR) Volterra model [5] are often employed. Recently, 2-D DPD model [6]-[7], 3-D tri-band DPD [8], frequency-selective DPD [9]-[10] have been proposed for multi-band systems. In general, these proposed DPD solutions work very well in existing systems and it has also been demonstrated that DPD is well feasible for FPGA (field-programmable gate array) and DSP (digital signal processor) implementation [11]-[14].

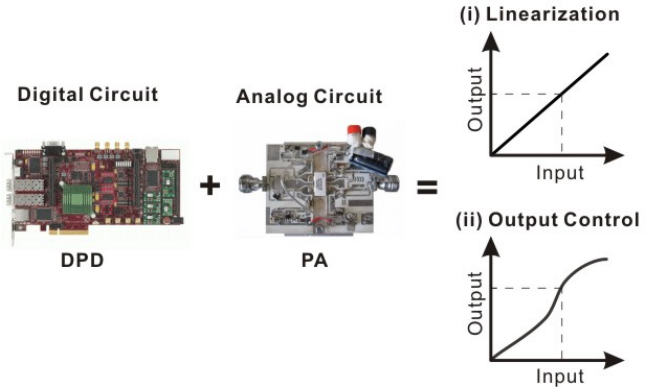

Fig.1. Digitally assisted analog design example: digital predistortion of power amplifier (i) Conventional linearization (ii) New output-controllable DPD.

The primary goal of DPD is accurately inversing the nonlinear behavior of the PA in order to obtain the linear performance of the transmitter. In other words, it aims to push the output signal of the PA to be exactly the same as the original input signal so that the input/output relationship is linear, as illustrated in Fig. 1(i). However, the scenario is gradually changing with the development of wireless communications systems. Various practical applications can be listed here as examples. For instance, in some transmitters, power efficiency can be much more crucial than linearity requirement. In order to obtain higher efficiency, part of linearity may have to be sacrificed which results that the final input/output may be no longer linear, as shown in Fig. 1(ii). In long term evolution-advanced (LTE-A) system, concurrent multi-band power amplifiers will be commonly deployed and resource blocks (RBs) in data frame will be dynamically assigned according to real-time data traffic. The data transmitted at each band may be generated from different users and using different modulation schemes. This implies that different linearity specifications might be required for each band separately. These scenarios' evolution will impose new challenges for digital predistortion over the conventional goal, that is, pushing the output to be the same as the original input is no longer applicable. DPD should be evolved to accommodate these specific scenarios. Then, one valuable question will be asked if the existing DPD systems can be easily adapted to these new

This work was supported by the Science Foundation Ireland under the Principal Investigator Award Scheme. This paper is an expanded version from IEEE MTT-S International Workshop on Integrated Nonlinear Microwave and Millimetre-wave Circuits (INMMiC), Leuven, Belgium, April 2-4, 2014.

The authors are with the School of Electrical, Electronic and Communications Engineering, University College Dublin, Dublin 4, Ireland (e-mail: chao.yu@ucdconnect.ie; michelallegue@gmail.com; yan.guo.1@ucdconnect.ie;anding.zhu@ucd.ie).

applications. The answer is no, because the principle that supports the existing DPD, i.e., the conventional *p*th-order inverse theory [15]-[16], is no longer valid, if the desired PA output is not equal to the original input. Therefore, it is necessary to develop new approaches to meet the new requirements.

In order to resolve this issue, a novel frequency component controllable DPD technique was proposed to realize single-band linearization in a tri-band system [17]. Because it is difficult to generate the partial inverse function directly, this approach adopts a different way. It is first to split the desired function into two cascaded sub-models that can be identified separately, and then combine them together to accurately form the whole partial inverse function. Due to limited space, only the basic idea was illustrated in [17]. In this paper, we further develop the proposed idea with in-depth theoretical analysis and extend the frequency component controllable method to a more comprehensive technique referred to as output-controllable partial inverse DPD. It is worth mentioning that the band-limited *p*th-order inverse theory [18] will be utilized in the identifications of the sub-models, which provides more bandwidth flexibilities in the practical system. Furthermore, the applications based on the proposed method have been extended to various interesting scenarios with experimental demonstrations, which validate the potential of the proposed method.

The rest of the paper is organized as follows: In Section II, the existing DPD is briefly reviewed and the limitation of the existing techniques will be pointed out. In Section III, the proposed DPD technique will be developed in detail with its implementation outlined in Section IV. Four interesting test cases along with experimental results are presented in Section V, with a conclusion given in Section VI.

II. Conventional Nonlinear Inverse

The principle of digital predistortion is based on nonlinear inverse. As illustrated in Fig. 2, the transmit signal is pre-processed by the DPD block before entering the power amplifier. If the transfer function of the DPD is the exact inverse of that of the PA, the final output signal will be linearly amplified. One of the key issues in DPD design is how to accurately identify the inverse function. In existing DPD systems, two model extraction structures, indirect learning and direct learning, are commonly employed. The indirect learning [19]-[20], also referred as the *p*th-order inverse [16], is based on the assumption that the *p*th-order pre-inverse of the system

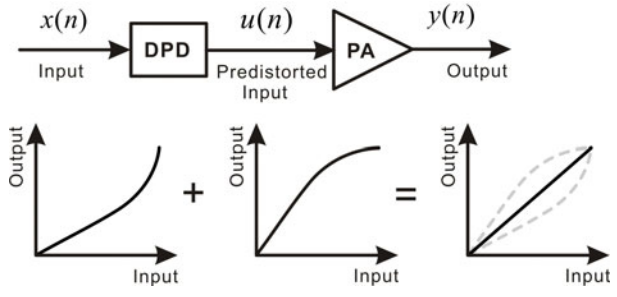

Fig.2. Conventional DPD system.

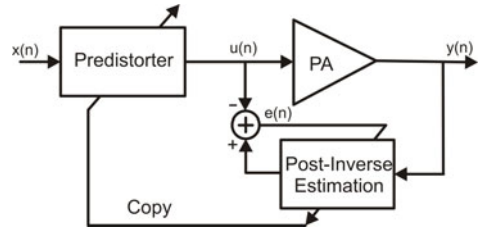

Fig. 3. Indirect learning architecture.

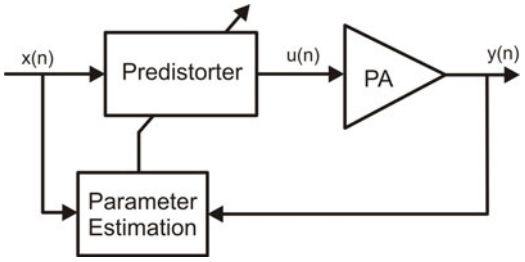

Fig. 4. Direct learning architecture.

is identical to its *p*th-order post-inverse if linearized up to *p*th-order nonlinearities. This is reasonable because the nonlinearities beyond *p*th-order (if p is a large number) are normally to be negligible in a real system. This leads that we can use an identical model for representing both the predistorter (pre-inverse) and the postdistorter (post-inverse), as illustrated in Fig. 3. During the model extraction process, the input and output of the PA are swapped, namely, the output of the PA is used as the input, and the input of the PA as the expected output, to first extract the post-inverse model of the PA, and then the extracted parameters are directly copied to the pre-inverse (DPD) block to carry out the predistortion. The direct learning [21], also referred as the model reference [22], is to extract the model via directly updating the coefficients using the errors between the original input and the final output of the PA, as shown in Fig. 4. Nevertheless, in the existing systems, either indirect learning or direct learning, the target is clear, namely, the optimum model is obtained when the minimum error between the input and the output is reached. In other words, the output of the PA, $y(n)$, is pushed close to the original input $x(n)$, and two cascaded systems, DPD and PA, exactly inverse each other.

However, with further development of wireless systems, some new scenarios will emerge. As mentioned earlier, for instance, some distortion in the output may remain after DPD for the sake of improving power efficiency of the PA. This leads that the desired PA output $y(n)$ is no longer expected to be the same as the original input $x(n)$. In other words, the input/output relationship of the cascaded system is

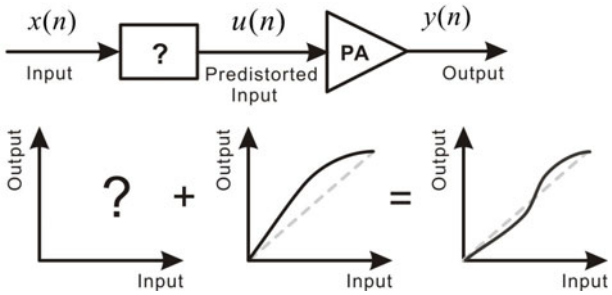

Fig. 5. The new scenario for the output-controllable DPD.

not necessarily exactly linear any more, as shown in Fig. 5. Under these situations, the conventional nonlinear inverse, either direct or indirect learning, is no longer applicable because the exact inverse is not useful any more. In consequence, a new approach must be developed to linearize the system under the new scenarios.

III. Output-Controllable Partial Inverse

In order to resolve the problem described above, an output-controllable partial inverse digital predistortion technique is proposed in this section.

A. Transfer Function Decomposition

The reason why we cannot directly derive the DPD function under the new scenarios is that the target output reference is no longer the original input, namely,

$$y(n) \neq x(n). \tag{1}$$

Therefore, the desired DPD function is no longer the exact inverse of that of the PA, i.e.,

$$H^{-1}H \neq 1. \tag{2}$$

It creates difficulties in finding H^{-1}, because the reference is no longer available. However, if we insert another nonlinear box, H_{target}, before the DPD, to generate the desired output $v(n)$ to match $y(n)$, e.g.,

$$y(n) = v(n), \tag{3}$$

the exact inverse

$$H^{-1}H = 1. \tag{4}$$

can be employed again, as shown in Fig. 6a. This simple concept not only resolves the model inverse problem described above, but also, more importantly, gives us much more freedom to control the output of the PA by using digital signal processing techniques, as demonstrated later.

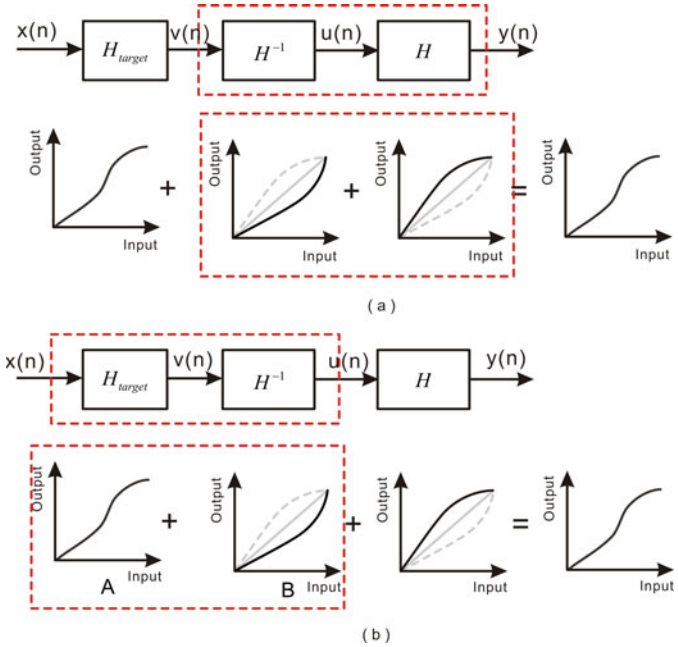

Fig. 6. Transfer function decomposition.

Comparing to the existing DPD system, we could treat these two boxes being decomposed from the original DPD function: H_{target} is used to generate the target output and H^{-1} is the exact inverse of the PA. The two functions can be identified separately, and after model extraction they can be combined and implemented in digital circuits together. Because the complete system, from the input to the output, is not exactly inversed, we can define this new predistortion process as *partial inverse*,

$$H_{partial}^{-1} = H_{target}H^{-1}, \tag{5}$$

as illustrated in Fig. 6b.

B. Target Model Generation

In this part, we will discuss how to use the target model H_{target} to control the PA output. Here, two types of control will be examined and the combination of two will also be considered.

(i) Linearization Level Control

Firstly, we discuss linearization level control for single-band systems. As mentioned earlier, in the existing DPD system, the main goal is aiming to remove all the distortion induced by the PA. However, in order to achieve higher power efficiency, it is not always possible to clean up all the distortion. In other words, linearity compromise must be made in return of higher efficiency in many cases. In the existing DPD, the brute force method would be to allow the DPD to linearize the PA to a certain distortion level and then focus on pushing the PA to achieve high power efficiency. This approach is simple and works reasonably well in general, but this blind approach cannot guarantee the optimum result is achieved because we do not have any insight information. For example, for a Doherty PA, the AM-AM curve may appear as an "S" shape, shown in Fig. 7, which indicates that the distortion is generated from different power levels and affected by different part of the amplifier inside the box. If an existing DPD is employed, the PA may be linearized to a certain linearity level by monitoring the final spectrum regrowth, as shown in Fig. 8. Because we do not know the remaining distortion is caused by which part of the PA, we cannot guarantee the maximum efficiency can be achieved. For instance, under the same distortion, two different AM-AM curves may appear after DPD. Curve A may achieve a better efficiency than that of Curve B. With the existing approach, we cannot guarantee we linearize the PA to Curve A.

However, if we can control how the PA behaves or clearly know what distortion will remain during the DPD process, we

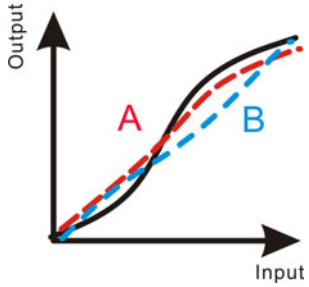

Fig. 7. AM-AM curves of a Doherty PA before and after DPD (Curve A: higher efficiency case; Curve B: lower efficiency case).

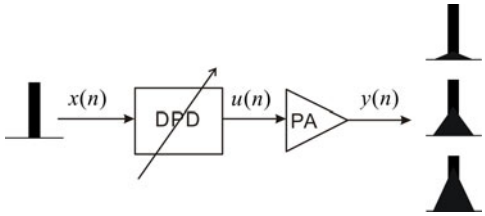

Fig. 8. Linearization output control.

can achieve the goal more objectively. For instance, we can use the target model proposed in Fig. 6 to generate the desired AM-AM curve, e.g., Curve A, in advance, and then conduct the complete inverse of the PA nonlinear behavior. We can then finally achieve Curve A in the output, and thus guarantee the PA reaches better efficiency.

In order to realize this target, we propose a technique called nonlinearity injection, by which the desired nonlinear distortion can be injected into the original input signal on purpose, as shown in Fig. 9. The output of the target model can be obtained by using

$$v(n) = x(n) + d(n), \tag{6}$$

where $d(n)$ represents the injected nonlinear terms, which could be generated from the original input $x(n)$ using a nonlinear equation,

$$d(n) = K[x(n)] = \sum_{p=2}^{P} K_p[x(n)], \tag{7}$$

where K_p is the nonlinear operator and P is nonlinear order. By employing the technique, a desired PA output can be generated.

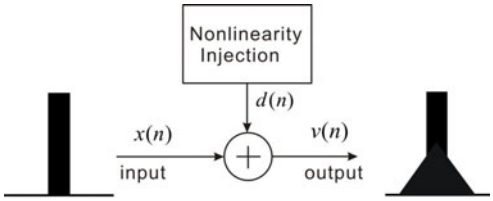

Fig. 9. Nonlinearity injection technique for the target model generation.

(ii) Linearization Band Control

The second type of control for manipulating the DPD output is referred to as linearization band control, in which the linearized frequency band and modulation bandwidth can be arbitrarily selected. This operation is very important for future concurrent multi-band systems. As we discussed in the introduction, concurrent multi-band amplifiers will be widely employed in LTE-A systems. In Fig. 10, we take a concurrent tri-band transmitter as an example, where the data transmitted in Band 1 may be modulated with a 16 Quadrature Amplitude Modulation (QAM) while Band 2 and Band 3 are modulated by

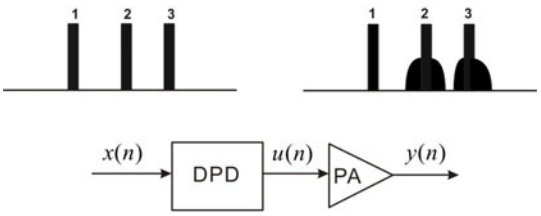

Fig. 10. Linearization of multi-band transmitters.

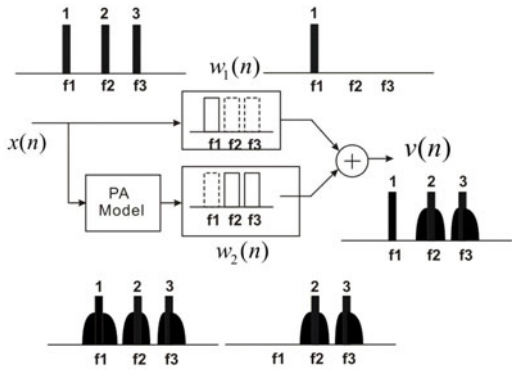

Fig. 11. Linearization band control for the target model generation.

Quadrature Phase Shift Keying (QPSK). The QAM modulation scheme is more sensitive to distortions than the QPSK modulation scheme because of its multi-level constellation nature while a QPSK keeps the constellation points in a constant magnitude ring over the complex plane. This leads that different linearity specifications might be required for each band depending on the modulation and/or coding schemes employed in the baseband for each band. For instance, in some cases, we might only need to linearize Band 1, but leave Band 2 and Band 3 untouched.

In order to realize this flexibility, we propose a linearization band selection technique for multi-band signals as shown in Fig. 11. Firstly, we use the PA behavioral model H to rebuild the PA output. Both the original input and the reconstructed output are sent to the band selection module to decide which bands are required to be linearized. Finally, they are combined together to form the target output as

$$v(n) = x(n) * w_1(n) + H[x(n)] * w_2(n), \tag{8}$$

where $w_1(n)$ and $w_2(n)$ represents the band selection function for the input and the reconstructed output.

The linearization level control and the linearization band control can be combined together to form a target model generation, as illustrated in Fig. 12 and described by,

$$v(n) = x(n) * w_1(n) + d(n) + H[x(n)] * w_2(n) \tag{9}$$

Using this combination, the capability of the proposed model can be largely improved and thus it is able to be flexibly configured and perform more complex functionalities.

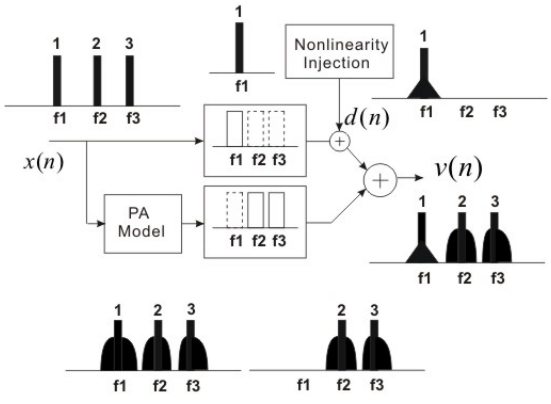

Fig. 12. Combined control in the target model generation.

C. Band-limited Model Inverse

After generating the target model, next step is to construct the inverse function H^{-1}. At a first glance, this model generation process should have no difference from that of the existing DPD. However, due to an additional nonlinear box, the target model, is added in the system and more complex signal processing is involved, there are certain constraints that must be considered in the model inversion process.

As we know that, in digital predistortion, when the input signal passes the DPD block, the bandwidth will be expanded, usually five times, due to nonlinear process of the signal. It means that the transmitter system should support at least five times the input signal bandwidth in order to keep high linearity performance. For example, in order to linearize a 40 MHz signal, at least 200 MHz bandwidth is required. As described earlier, under the new scenario, there is an additional nonlinear module, the target model, before the model inverse. The signal bandwidth will also be expanded after passing the target model. Although the bandwidth of the final output may be reversed, bandwidth will be expanded significantly in interim when the signal is passing through the two cascaded boxes. If we take a 40 MHz signal as an example, the output of the target model can be 200 MHz if the nonlinearity is set to fifth order and then, the predistorted signal will be further five times that bandwidth, that is, 1000 MHz, as illustrated in Fig, 13a. The bandwidth expansion will be much more severe when the technique is applied to a multi-band system, as shown in Fig. 13b.

Therefore, the bandwidth expansion issue must be carefully considered when constructing the DPD model. Fortunately, a band-limited DPD technique was introduced in [18], in which the bandwidth constraints of DPD system can be removed without sacrificing linearization performance. This technique provides a very effective way to manipulate and control the signal bandwidth in DPD modeling. In this work, we adopt the band-limited DPD technique in constructing the new DPD model. In order to control the signal bandwidth in each module, we can insert a band-limiting function into each transfer function to control the signal bandwidth, as shown in Fig. 14. Then the new transfer functions can be defined as

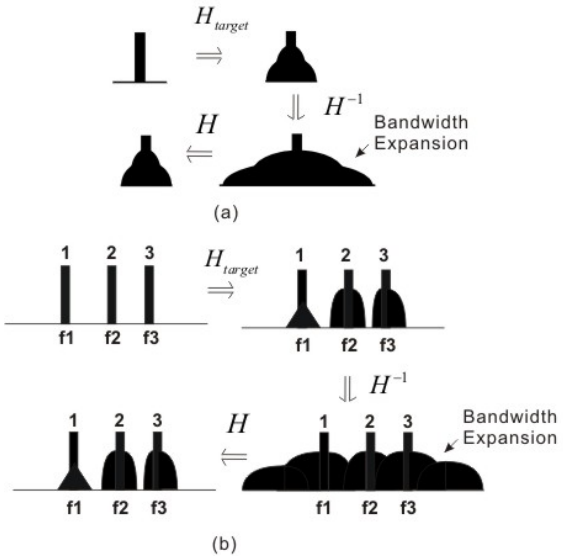

Fig. 13.Bandwidth expansion: (a) single-band system; (b) multi-band system.

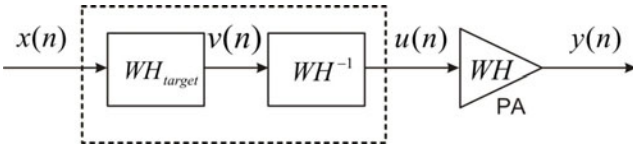

Fig. 14. Bandwidth consideration for the proposed system.

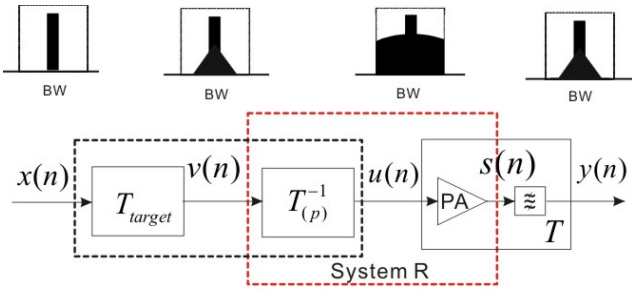

Fig. 15. Illustration of a band-limited system.

$$T_{target} = WH_{target}. \tag{10}$$

$$T^{-1} = WH^{-1} \tag{11}$$

The band-limited PA system can be realized by cascading the PA with a band-pass filter, which has been discussed in [18], that is,

$$T = WH. \tag{12}$$

Therefore, the system illustrated in Fig. 14 can be modified to the new system illustrated in Fig. 15, in which only the nonlinearities below *p*th-order are considered. Therefore, the partial inverse function can be built by using these two band-limited transfer functions,

$$H_{partial}^{-1} = T_{target} T_{(p)}^{-1}, \tag{13}$$

Considering the system *R* in Fig. 15, the PA output $s(n)$ can be constructed as

$$s(n) = H\left[(T)_{(p)}^{-1}[v(n)]\right] = v(n) + \sum_{i=p+1}^{\infty} R'_{(i)}[v(n)] + \sum_{i=1}^{\infty} R''_{(i)}[v(n)], \tag{14}$$

where $R'_{(i)}$ and $R''_{(i)}$ are the *i*th-order band-limited Volterra operator within and out of the specified bandwidth of the cascaded system *R*, respectively. Because

$$v(n) = T_{target}[x(n)], \tag{15}$$

Substituting(15) into (14), we can obtain:

$$s(n) = T_{target}[x(n)] + \sum_{i=p+1}^{\infty} R'_{(i)}[T_{target}[x(n)]] + \sum_{i=1}^{\infty} R''_{(i)}[T_{target}[x(n)]]. \tag{16}$$

Finally, with the assist of the band-pass filter, the output $y(n)$ can be obtained as:

$$y(n) = T_{target}[x(n)] + \sum_{i=p+1}^{\infty} R'_{(i)}[T_{target}[x(n)]]. \tag{17}$$

It is worth mentioning that if the bandwidth of $v(n)$ does not exceed the specified bandwidth, the band-pass filter after PA could be removed without affecting the performance. That is because

$$\sum_{i=1}^{\infty} R''_{(i)}[T_{target}[x(n)]] = 0. \tag{18}$$

IV. DPD Implementation

In this section, we will discuss how the complete DPD system is implemented.

A. Model Selection

In this proposed approach, it requires three behavioral models in the system: a PA model (the forward model), a DPD model (the inverse model) and a nonlinearity injection model. The model selection depends on the system requirement. In this work, we employ the band-limited second-order DDR-Volterra model [18] for both the forward and the inverse models. The model function can be expressed as,

$$\begin{aligned} y(n) = & \sum_{p=0}^{(P-1)/2}\sum_{i=0}^{M} g_{2p+1,1,BL}(i)\left[\sum_{k=0}^{K}|u(n-k)|^{2p}\,u(n-i-k)w(k)\right] \\ & + \sum_{p=1}^{(P-1)/2}\sum_{i=1}^{M} g_{2p+1,2,BL}(i)\left[\sum_{k=0}^{K}|u(n-k)|^{2(p-1)}\,u^2(n-k)u^*(n-i-k)w(k)\right] \\ & + \sum_{p=1}^{(P-1)/2}\sum_{i=1}^{M} g_{2p+1,3,BL}(i)\left[\sum_{k=0}^{K}|u(n-k)|^{2(p-1)}\,u(n-k)\,|u(n-i-k)|^2\,w(k)\right] \\ & + \sum_{p=1}^{(P-1)/2}\sum_{i=1}^{M} g_{2p+1,4,BL}(i)\left[\sum_{k=0}^{K}|u(n-k)|^{2(p-1)}\,u^*(n-k)u^2(n-i-k)w(k)\right] \end{aligned} \tag{19}$$

where $y(n)$ and $u(n)$ are the PA output and input, $w(n)$ represents the baseband band-limiting function, which can be defined by the system bandwidth. $g_{2p+1,j,BL}(\cdot)$(j=1, 2, 3, 4) are the coefficients of the band-limited model. P is the odd nonlinearity order, M is the memory length, and K is the length of the band-limiting function. To increase modeling accuracy, the decomposed piecewise technique [23] may be used.

For simplicity, the model can be constructed in matrix form, that is

$$\mathbf{Y}_{\mathbf{N}\times 1} = \mathbf{U}_{\mathbf{N}\times\mathbf{L}}\mathbf{C}_{\mathbf{L}\times 1}, \tag{20}$$

where $\mathbf{Y}$ is the output vector generated from the PA output, $\mathbf{U}$ is the input matrix generated from PA input, containing all linear and nonlinear terms appearing in the input. $\mathbf{C}$ is the coefficients vector. N is the number of data samples and L is the number of coefficients.

Both the forward model and the inverse model of the PA can be constructed by using the same model structure in (20). To distinguish the two models, superscripts are used on the matrix/vector symbols. The forward model use the PA input and output to build the input matrix $\mathbf{U}^{(1)}$ and the output vector $\mathbf{Y}^{(1)}$, while in the inverse model, the input and the output are swapped, that is, we use the PA input to build the output vector $\mathbf{U}^{(2)}$, and the PA output to build the input matrix $\mathbf{Y}^{(2)}$, which can be expressed as

$$\begin{cases} \mathbf{Y}^{(1)}_{\mathbf{N}\times 1} = \mathbf{U}^{(1)}_{\mathbf{N}\times\mathbf{L}_1}\mathbf{C}^{(1)}_{\mathbf{L}_1\times 1} \\ \mathbf{U}^{(2)}_{\mathbf{N}\times 1} = \mathbf{Y}^{(2)}_{\mathbf{N}\times\mathbf{L}_2}\mathbf{C}^{(2)}_{\mathbf{L}_2\times 1} \end{cases} \tag{21}$$

where $\mathbf{C}^{(1)}_{L_1\times 1}$ and $\mathbf{C}^{(2)}_{L_2\times 1}$represents the coefficients vector of the forward model and the inverse model, respectively. Because these two models usually have different numbers of coefficients, therefore, we use L_1 and L_2 to represent the coefficients length separately. Since the model is linear-in-parameters, we can employ linear identification algorithms, such as least squares (LS), for model extraction, i.e.,

$$\begin{cases} \mathbf{C}^{(1)}_{\mathbf{L}_1\times 1} = \left(\left(\mathbf{U}^{(1)\mathbf{H}}\right)_{\mathbf{L}_1\times\mathbf{N}}\mathbf{U}^{(1)}_{\mathbf{N}\times\mathbf{L}_1}\right)^{-1}\left(\mathbf{U}^{(1)\mathbf{H}}\right)_{\mathbf{L}_1\times\mathbf{N}}\mathbf{Y}^{(1)}_{\mathbf{N}\times 1} \\ \mathbf{C}^{(2)}_{\mathbf{L}_2\times 1} = \left(\left(\mathbf{Y}^{(2)\mathbf{H}}\right)_{\mathbf{L}_2\times\mathbf{N}}\mathbf{Y}^{(2)}_{\mathbf{N}\times\mathbf{L}_2}\right)^{-1}\left(\mathbf{Y}^{(2)\mathbf{H}}\right)_{\mathbf{L}_2\times\mathbf{N}}\mathbf{U}^{(2)}_{\mathbf{N}\times 1} \end{cases} \tag{22}$$

The nonlinearity injection model can also be any behavioural models. In this work we use a simple polynomial function as an example, as demonstrated in Section V.

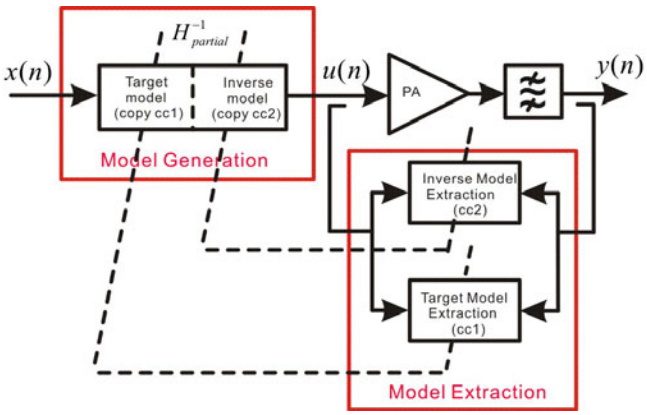

Fig. 16. Structure of the proposed output-controllable DPD.

B. The Full System Structure

Fig. 16 shows the complete structure of the proposed DPD system. In this new structure, the model generation module is divided into two parts, including target model and inverse model. The model extraction module also includes two parts: inverse model extraction and target model extraction.

Before the system starts, the input and output data from the PA without DPD must be captured and a target model is then constructed. For linearization level control, a nonlinearity injection model needs to be selected. For frequency band control, the forward PA model must be extracted and the filtering functions must be selected, and then the target model can be generated as shown in Fig. 11. For combined control, the target model can be constructed as shown in Fig. 12. The original input is then sent to the target model to generate the desired output and fed to the PA to generate the new output. The target model output and the final PA output are then used for the inverse model extraction, as that is usually conducted in the existing DPD, e.g., indirect learning [20]. The model extraction process can be conducted in several iterations. The nonlinearity injection function is directly related to the PA linearity and power efficiency. It may need to be changed and tuned many times before achieving the best performance.

V. Experimental Validations

In order to validate the proposed method, we tested a high power LDMOS Doherty PA with the center frequency at 2.14 GHz in four cases:(1) Linearization level control with spectrum mask;(2) Linearization band control in a tri-band system; (3)

Linearization band control with sideband compensation; and (4) Combined control.

The test bench was setup as shown in Fig. 17. The signal source was generated in baseband from the software MATLAB in PC, then sent into the baseband board, up-converted by the RF board to 2.14 GHz, and finally fed into the PA. In the feedback observation path, the system bandwidth was set to 140 MHz and the Analog-to-digital converter (ADC) sampling rate is 368.64 MSPS (mega samples per second) for IF sampling. The band-limited decomposed piecewise 2nd-order DDR model [18] was employed for both the PA forward and inverse models and the model configuration depended on the application cases.

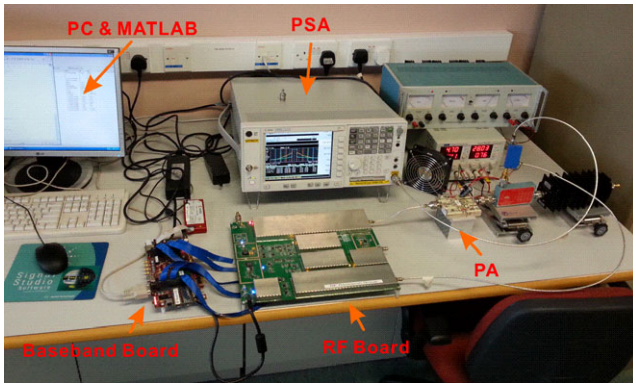

Fig. 17. The test bench setup.

A. Linearization Level Control with Spectrum Mask

In this application, a 4-carrier 20 MHz WCDMA signal with peak-to-average power ratio (PAPR) of 6.5 dB was used as the test signal. Without DPD, the power amplifier introduced strong nonlinearity and memory effects, as shown in the AM-AM and AM-PM curves in Fig. 18. In the DPD model configuration, the magnitude threshold was set as 0.5 for the normalized data and the corresponding nonlinearity order was selected as {7, 7}. The memory length was set to {3, 3} to obtain the best performance. A digital filter with 140 MHz bandwidth was chosen to meet the bandwidth limitation in the feedback path. With the existing DPD, the nonlinearity and memory effects induced by the PA can be almost completely removed, as illustrated in Fig. 19.

To demonstrate how we evaluate the performance for linearization level control under different conditions, a 3rd-order polynomial function was employed for generating the nonlinearity injection signal, that is,

$$y(n) = x(n) + a|x(n)|^2 x(n), \tag{23}$$

where a is a tuning factor to build different spectrum mask and is set as 0, -0.1, -0.2, -0.3. Note that the function (23) above was used for a proof-of-concept demonstration only. In a real system, different function structures can be employed to create the desired spectrum emission masks for particular standards and tuned for particular amplifiers.

With different levels of nonlinearity injection, the linearization level changes accordingly. The output spectra in the frequency domain are shown in Fig. 19a while AM-AM curves are plotted in Fig. 19b.The performance summary of this test is listed in Table I, where we can see that the output power can be increased from the existing DPD output at 37.10 dBm to the new one (a=-0.1) at 37.80 dBm, and the corresponding drain efficiency (DE) is increased by 3%, from 28.62% to 31.65%. In the meantime, the corresponding adjacent channel power ratio (ACPR) is dropped from -56.65/-55.70 dBc to

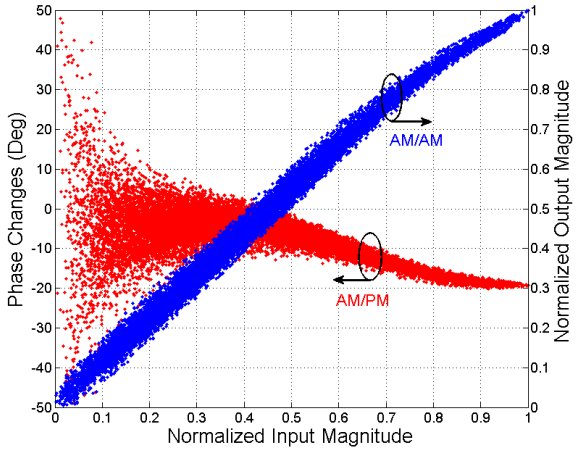

Fig. 18. Measured AM/AM and AM/PM characteristics of PA without DPD with the output power of 39.1 dBm

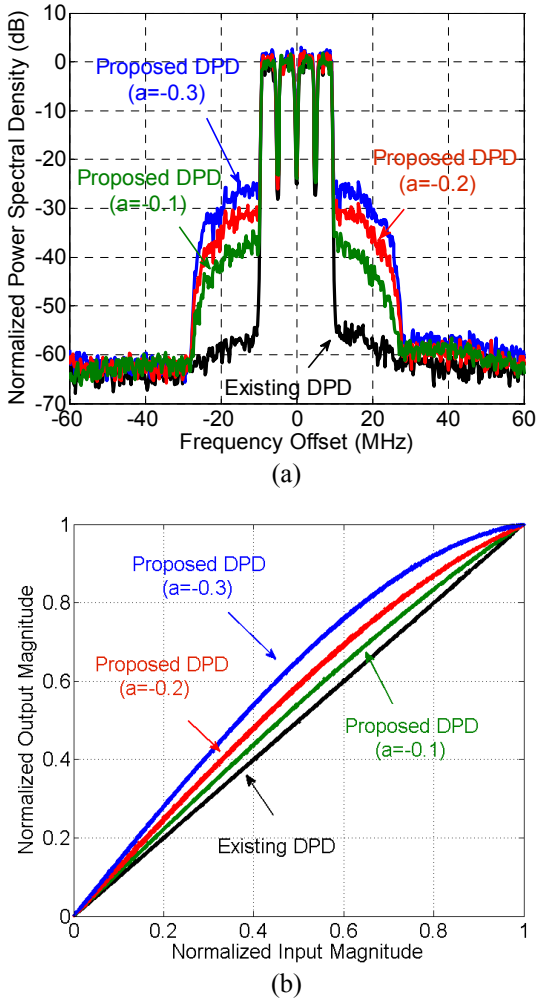

Fig. 19. Measured results with linearization level control after DPD: (a) frequency domain spectra (b) AM-AM curves.

TABLE I

SUMMARY OF THE PERFORMANCE IN LINEARIZATION LEVEL CONTROL

	Pout (dBm)	DE (%)	ACPR (±5 MHz) (dBc)		ACPR (±10 MHz) (dBc)		NRMSE0 (%)	NRMSE (%)
Without DPD	37.21	29.35	-30.24	-29.11	-32.55	-30.71	13.31	13.31
Existing DPD	37.10	28.62	-56.65	-55.70	-57.21	-56.19	0.64	0.64
Proposed DPD (a=-0.03)	37.38	30.06	-46.00	-47.15	-47.45	-50.05	0.65	0.99
Proposed DPD (a=-0.04)	37.43	30.40	-45.02	-45.74	-46.23	-48.88	0.52	1.15
Proposed DPD (a=-0.05)	37.50	30.43	-42.06	-43.11	-43.69	-45.44	0.71	1.44
Proposed DPD (a=-0.1)	37.80	31.65	-36.42	-37.70	-38.45	-40.06	0.75	2.66
Proposed DPD (a=-0.2)	38.46	34.79	-30.22	-31.06	-32.34	-33.10	0.46	5.22
Proposed DPD (a=-0.3)	39.17	37.82	-26.41	-27.22	-28.54	-29.18	0.59	8.16

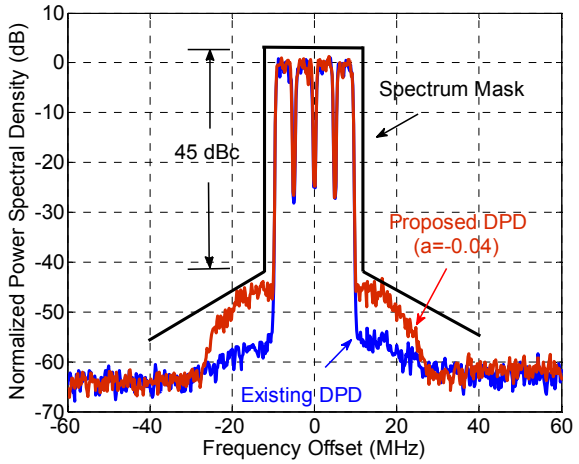

Fig. 20. Measured power spectral density under spectrum mask.

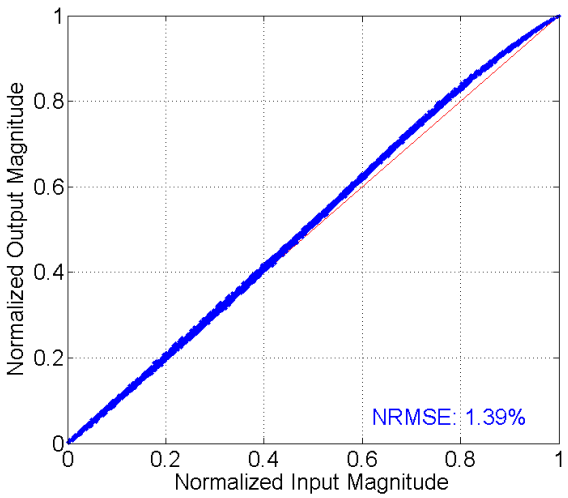

Fig. 21. Linearization level control with complex waveform.

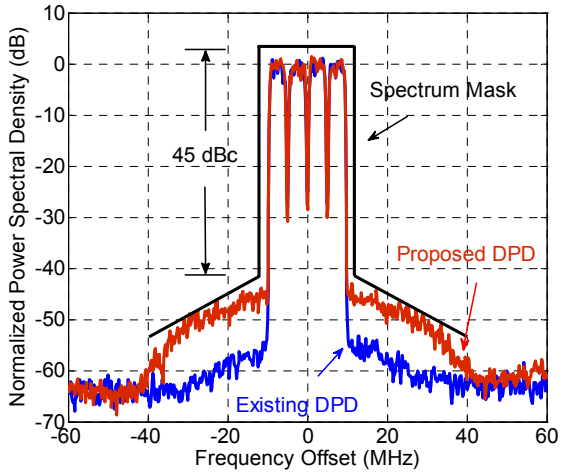

Fig. 22. Measured power spectral density under spectrum mask of the complex waveform.

-36.42/-37.70 dBc with the frequency offset of ±5 MHz, respectively. From the results, we can see that, by employing the proposed method, a trade-off between the efficiency and the linearity can be made. For instance, if there is a spectrum mask with -45 dBc of ACPR requirement, shown in Fig. 20, we can choose a = -0.04 for the linearization level control to allow the PA to be linearized to -45.02/-45.74 dBc of ACPR while keep the drain efficiency at 30.40%, increased by almost 2% from 28.62% achieved from the complete inverse (the existing DPD).

Table I also gives the NRMSE (normalized root mean square error) values. The values in "NRMSE0" column are calculated from comparing the final PA output $y(n)$ with the target output $v(n)$. Small values appeared in this column indicate that the inverse model (DPD block) works very well. The values in the "NRMSE" column are obtained from comparing the final PA output with the original input $x(n)$, where we can see that the NRMSE proportionally increases with the level of nonlinearity injection. This is not surprising because the nonlinearity injection function (23) introduces both in-band and out-of-band distortion. From the results, we can see that there are only moderate increases on NRMSE values, which usually can be ok.

As mentioned earlier, (23) is used for an example only and different nonlinearity injection functions can be employed according to the practical requirements. For instance, instead of using (23), the following nonlinear function

$$y(n) = x(n) + 0.1x(n-1) + 0.19|x(n)|^2 x(n) - 0.19|x(n)|^4 x(n) \quad (24)$$

can also be employed, where not only the terms with higher nonlinearity orders but also the memory terms are included. The AM-AM plot of the final PA output verse the original input is shown in Fig. 21. In this case, the drain efficiency is 30.82% and the out-of-band distortion can still be kept under the spectrum mask as shown in Fig. 22, but the NRMSE is increased to 1.39% because of increased nonlinearity and additional memory effects. Furthermore, the in-band distortion can be controlled separately from the out-of-band distortion if required.

B. *Linearization Band Control in a Tri-band system*

In this application, the linearization band control is evaluated in a tri-band system, in which the signal bands can be arbitrarily chosen to be linearized. In order to validate this idea, the PA was excited by a tri-band signal with PAPR of 8.1 dB and each band has a 5 MHz bandwidth. In the model configuration, the target model is constructed as shown in Fig. 11 and the mathematical expression is shown in (8). For the PA forward model $H(\cdot)$, the band-limited second-order piecewise DDR-Volterra model is employed, where the magnitude threshold was set as 0.5 for the normalized data, the corresponding nonlinearity order was selected as {7, 7} and the memory length was set to {5, 5}. Three digital filtering functions are used for the three bands, one for each band. For band 1, the bandwidth is set from -20 ~ -15 MHz.

TABLE II

SUMMARY OF THE LINEARIZATION PERFORMANCE FOR TRI-BAND SIGNAL

Linearization Scenario		Pout (dBm)	DE (%)	ACPR(±5MHz) (dBc)	NRMSE (%)
Without DPD	B1&B2&B3*	37.59	31.54	-31.2&-30.5 &-30.9	12.3&9.2 &12.4
With DPD	B1	37.81	32.68	-58.4	0.8
	B2	37.61	31.69	-59.2	0.6
	B3	37.59	31.54	-58.7	0.5
	B1&B2	37.33	30.18	-58.6&-58.1	1.1&1.2
	B1&B3	36.83	28.22	-55.4&-54.6	1.3&1.1
	B2&B3	37.39	30.60	-57.3&-57.8	0.8&1.0
	B1&B2&B3	37.09	29.47	-59.9&-59.0 &-58.8	0.9&1.0 &1.3

*B1:Band 1(-20~-15 MHz); *B2:Band 2(0~5 MHz); *B3:Band 3(15~20 MHz)

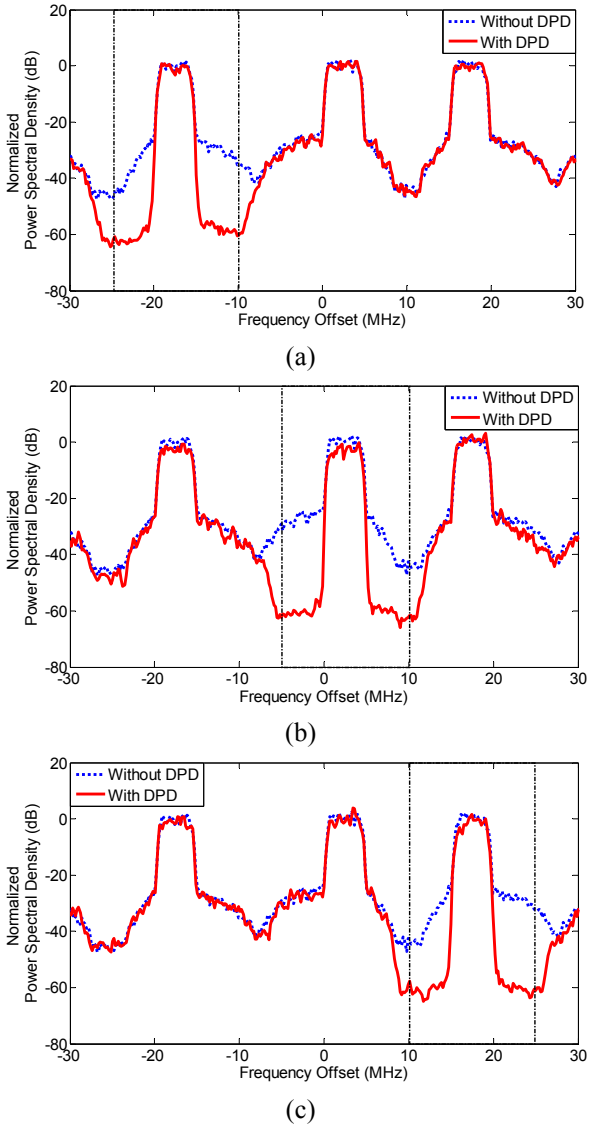

Fig. 23. Measured linearization performance for single band: (a) band 1, (b) band 2, and (c) band 3.

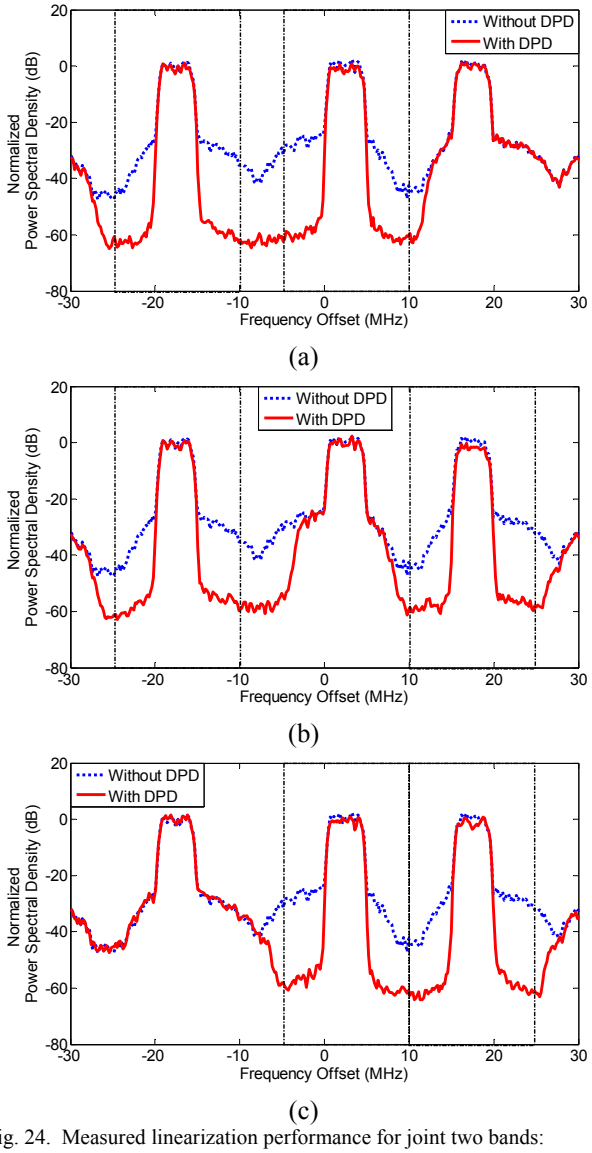

Fig. 24. Measured linearization performance for joint two bands: (a) band 1&2, (b) band 1&3, and (c) band 2&3.

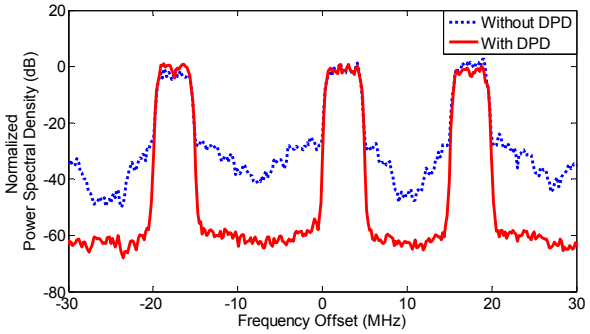

Fig. 25. Measured linearization performance for joint three bands.

For band 2, bandwidth is set from 0 ~ 5 MHz. For band 3, the bandwidth is set from 15 ~ 20 MHz. In these three bands, the ones expected to be linearized are combined together to construct $w_1(\cdot)$, while the others are used to form $w_2(\cdot)$. For the PA inverse model, all the parameter are the same as the ones of PA forward model, except that the memory length was set differently, that is {4, 4}, to obtain the best performance. A digital filter with 140 MHz bandwidth was chosen to meet the bandwidth limitation in the feedback path.

The measured results are shown in Figs. 23-25. From Fig. 23, although the scenario is severe, the excellent linearization performance for each band can still be obtained. Later, the joint linearization performance for arbitrary two bands as shown in Fig. 24 and three bands as shown in Fig. 25 are very similar to those shown in Fig. 23. Table II gives the summary of the linearization performance for the tri-band signal.

C. Linearization Band Control with Sideband Compensation

In this application, we try to control the sideband compensation. A dual-band signal with PAPR of 7.8 dB was employed. The bandwidth spacing is 35 MHz. Fig. 26 shows the measured linearization performance for each sideband. From Fig. 26, the distortion in each sideband can be effectively compensated without affecting other bands. Table III gives a summary for the performance of sideband compensation in the dual-band signal, which can be evaluated by CIMPR (carrier-to-intermodulation-products power ratio). In Table III, the CIMPR was improved by more than 30 dB, reaching -60 dBc.

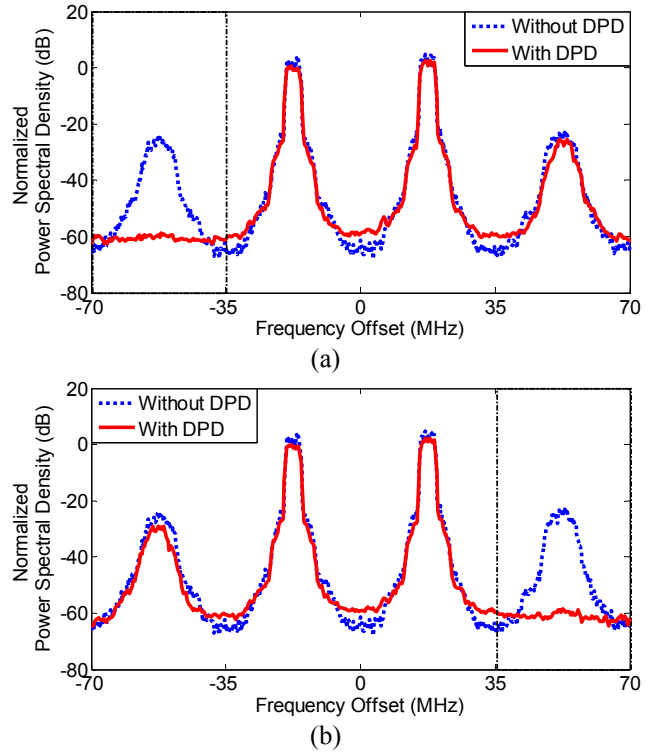

Fig. 26. Measured performance for sideband compensation. (a) left sideband compensation (b) right sideband compensation

TABLE III
SUMMARY OF THE PERFORMANCE FOR SIDEBAND COMPENSATION

Linearization Scenario	Pout (dBm)	DE (%)	CIMPR (dBc)	
			LS	RS
Without DPD	37.70	31.86	-27.8	-27.5
With DPD (LS*)	37.62	31.76	-59.1	N/A
With DPD (RS*)	37.34	30.25	N/A	-60.4

*LS: left sideband, RS: right sideband

D. Combined Control

In this application, we combine the validated two types control method to perform more complex functionality. The same signal as set in Part C was employed again. For linearization lever control, these two bands were configured separately to evaluate the capability of the proposed model, e.g., for the right band,

$$y(n)=x(n)-0.4|x(n)|^2x(n)+0.9|x(n)|^4x(n), \quad (25)$$

and for the left band,

$$y(n)=x(n)+0.3|x(n)|^2x(n)-0.7|x(n)|^4x(n). \quad (26)$$

Both the output waveforms were designed to meet the defined 45 dBc spectrum mask in frequency domain.

Fig. 27 shows the measured input/output relationship. The measured results validate the capability of the proposed model to build complex waveform for each band. Fig.28 shows the measured normalized power spectral density. From Fig. 28, we can find that these two bands can meet the pre-defined spectrum mask while realizing the complex input/output relationship as shown in Fig. 27. The detailed performance is listed in Table IV. Finally, these tests validate that the proposed method has the capability of fully providing the flexibilities both in time and frequency domain to design the output waveform, according to the designers' demand.

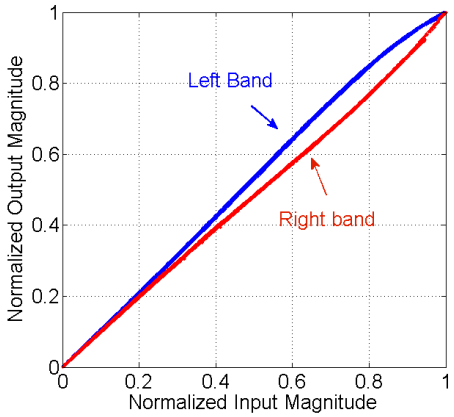

Fig. 27.Measured input/output relationship for left and right band in combined control

TABLE IV

THE PERFORMANCE OF COMBINED CONTROL

	Pout (dBm)	DE (%)	ACPR (±5 MHz) (dBc)	ACPR (±10 MHz) (dBc)	NRMSE (%)
			LB* / RB*	LB / RB	LB / RB
Without DPD	37.45	31.02	-32.35/-31.67	-52.85/-53.72	7.06/6.88
Existing DPD	36.92	28.34	-58.53/-59.39	-62.55/-61.95	0.75/0.77
Proposed DPD	36.96	28.61	-46.71/-47.87	-62.10/-61.16	1.00/1.47

*LB: left band, *RB: right band

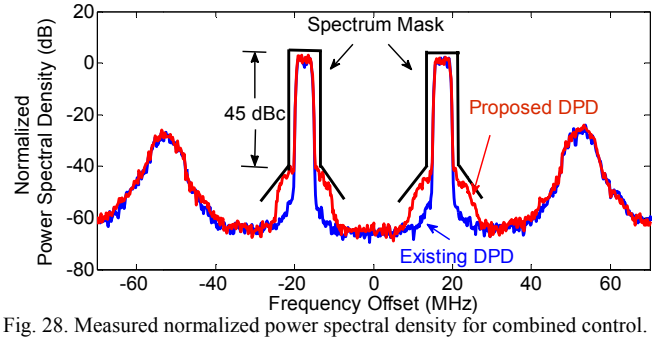

Fig. 28. Measured normalized power spectral density for combined control.

VI. CONCLUSION

In this paper, a novel output-controllable digital predistortion technique has been proposed to manipulate the output of RF power amplifiers according to user's demand. This is achieved by cascading a target model with a band-limited *p*th-order inverse model to partially inverse the nonlinear behavior of the PA. The proposed approach significantly expands the capability of existing digital predistortion and it provides more flexibility for system designers to conduct system optimization. Four practical applications were tested to validate the proposed method. The experimental results demonstrate that there are great potentials and benefits for this approach to be employed in current and future wideband wireless communication systems.

REFERENCES

[1] J. Kim, and K. Konstantinou, "Digital predistortion of wideband signals based on power amplifier model with memory," *Electron. Lett.*, vol. 37, no. 23, pp. 1417–1418, Nov. 2001.

[2] T. Liu, S. Boumaiza, and F. M. Ghannouchi, "Augmented Hammerstein predistorter for linearization of broadband wireless transmitters," *IEEE Trans. Microw. Theory Techn.*, vol. 54, no. 4, pp. 1340–1349, Jun.2006.

[3] D. R. Morgan, Z. Ma, J. Kim, M. G. Zierdt, and J. Pastalan, "A generalized memory polynomial model for digital predistortion of RF power amplifiers," *IEEE Trans. Signal Process.*, vol. 54, no. 10, pp. 3852–3860, Oct. 2006.

[4] F. M. Ghannouchi, and O. Hammi, "Behavioral modeling and predistortion," *IEEE Microwave Mag.,* vol. 10, no. 7, pp. 52-64, Dec. 2009.

[5] A. Zhu, P. J. Draxler, J. J. Yan, T. J. Brazil, D. F. Kinball, and P. M. Asbeck, "Open-loop digital predistorter for RF power amplifiers using dynamic deviation reduction-based Volterra series," *IEEE Trans. Microw. Theory Techn.*, vol. 56, no. 7, pp. 1524–1534, Jul. 2008.

[6] S. A. Bassam, M. Helaoui and F. M. Ghannouchi, "2-D digital predistortion (2-D-DPD) architecture for concurrent dual-band transmitters," *IEEE Trans. Microw. Theory Techn.*, vol. 59, no. 10, pp. 2547-2553, Oct. 2011.

[7] Y. Liu, W. Chen, J. Zhou, B. Zhou, and F. M. Ghannouchi, "Digital predistortion for concurrent dual-band transmitters using 2-D modified memory polynomials," *IEEE Trans. Microw. Theory Techn.*, vol.61, no.1, pp.281-290, Jan. 2013.

[8] M. Younes, A. Kwan, M. Rawat, F. M. Ghannouchi, "Linearization of concurrent tri-Band transmitters using 3-D phase-aligned pruned Volterra model," *IEEE Trans. Microw. Theory Techn.*, vol.61, no.12, pp.4569-4578, Dec. 2013.

[9] P. Roblin, S. K. Myoung, D. Chaillot, Y. G. Kim, A. Fathimulla, J. Strahler, and S. Bibyk, "Frequency selective predistortion linearization of RF power amplifiers," *IEEE Trans. Microw. Theory Techn.*, vol. 56, no. 1, pp. 65-76, Jan. 2008.

[10] J. Kim, P. Roblin, D. Chaillot, and Z. Xie, "A generalized architecture for the frequency-selective digital predistortion linearization technique," *IEEE Trans. Microw. Theory Techn.*, vol. 61, no. 1, pp. 596-605, Jan. 2013.

[11] P. L. Gilabert, A. Cesari, G. Montoro, E. Bertran, J-M. Dilhac, "Multi-lookup table FPGA implementation of an adaptive digital predistorter for linearizing RF power amplifiers with memory effects," *IEEE Trans. Microw. Theory Techn.*, vol. 56, no.2, pp.372,384, Feb. 2008.

[12] L. Guan, and A. Zhu, "Low-cost FPGA implementation of Volterra series-based digital predistorter for RF power amplifiers," *IEEE Trans. Microw. Theory Techn.*, Vol. 58, pp.866- 872, Apr. 2010.

[13] L. Guan, and A. Zhu, "Optimized low-complexity implementation of least squares based model extraction for digital predistortion of RF power amplifiers," *IEEE Trans. Microw. Theory Techn.*, vol.60, no.3, pp.594-603, Mar. 2012.

[14] P. L. Gilabert, G. Montoro, E. Bertran, "FPGA implementation of a real-time NARMA-based digital adaptive predistorter," *IEEE Trans. on Circuits and Systems II: Express Briefs*, vol.58, no.7, pp.402-406, Jul. 2011.

[15] M. Schetzen, "Theory of pth-order inverses of nonlinear systems", *IEEE Trans. on Circuits and Systems*, 23(5), 285-291, May 1976.

[16] M. Schetzen, *The Volterra and Wiener Theories of Nonlinear Systems*, reprint ed. Melbourne, FL: Krieger, 1989.

[17] C. Yu, M. Allegue-Martinez, and A. Zhu, "Frequency component controllable digital predistortion of RF power amplifiers,"*2014 International Workshop on Integrated Nonlinear Microwave and Millimetre-wave Circuits (INMMiC)*, pp.1-3, Leuven, Belgium, Apr. 2014.

[18] C. Yu, L. Guan, E. Zhu, A. Zhu, "Band-limited Volterra series-based digital predistortion for wideband RF power amplifiers," *IEEE Trans. Microw. Theory Techn.*, vol.60, no.12, pp.4198-4208, Dec. 2012.

[19] L. Ding, G. T. Zhou, D. R. Morgan, Z. Ma, J. S. Kenney, J. Kim, and C. R. Giardina, "A robust digital baseband predistorter constructed using memory polynomials," *IEEE Trans. Commun.*, vol. 52, no. 1, pp.159–165, Jan. 2004.

[20] C. Eun and E. J. Powers, "A new Volterra predistorter based on the indirect learning architecture," *IEEE Trans. Signal Process.*, vol. 45, no. 1, pp. 223–227, Jan. 1997.

[21] D. Zhou and V. E. DeBrunner, "Novel adaptive nonlinear predistorters based on the direct learning algorithm," *IEEE Trans. Signal Process.,* vol. 55, no. 1, pp. 120–133, 2007.

[22] P. Draxler, J. Deng, D. Kimball, I. Langmore, and P. M. Asbeck, "Memory effect evaluation and predistortion of power amplifiers," in *IEEE MTT-S Int. Dig.*, Long Beach, CA, Jun. 2005, pp. 1549–1552.

[23] A. Zhu , P. J. Draxler , H. Chin , T. J. Brazil , D. F. Kimball, and P. M. Asbeck, "Digital predistortion for envelope-tracking power amplifiers using decomposed piecewise Volterra series", *IEEE Trans. Microw. Theory Techn.*, vol. 56, no. 10, pp. 2237-2247, Oct. 2008.

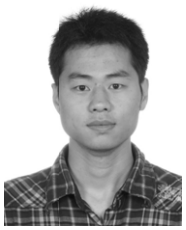

Chao Yu (S'09) received the B.E. degree in information engineering and M.E. degree in electromagnetic fields and microwave technology from Southeast University, Nanjing, China, in 2007 and 2010, respectively, and the Ph.D. degree in electronic engineering from University College Dublin (UCD), Dublin, Ireland, in 2014.

He is currently a research fellow in RF & Microwave Research Group, University College Dublin, Ireland. His research interests include RF power amplifiers modeling and linearization,

high-speed ADC correction, antenna design, FPGA hardware implementation and RF wireless system design.

Michel Allegue-Martínez received the Engineering Diploma in Telecommunications and Electronics from the Polytechnique Higher Institute "J.A. Echeverría" (ISPJAE), Havana, Cuba, in 2006 and the respective homologation by the Spanish Ministry of Education. He was granted with the MAEC-AECID merit-based scholarship by the Spanish Government in 2008. He received the MSc. and PhD. in Electronic, Signal Processing and Communications from the University of Seville in 2010 and 2012, respectively. He spent one year as a Senior Research Engineer in the University College Dublin (UCD) in a technology transfer project with the European Space Agency (ESA). His research interests are the nonlinear behavioral modeling of quadrature modulators, power amplifiers and other microwave subsystems, the compensation of linear and nonlinear impairments in wireless communication systems and satellite links, and the FPGA prototyping of advanced digital processing techniques. He was recipient of the "2011-2012 Ph.D. Thesis Extraordinary Award" from the University of Seville.

Yan Guo (S'13) received the B.E. degree in Information Science and Engineering from East China Jiaotong University in 2007 and the M.E. degree in Communication and Information Systems from Southeast University in 2011. He is currently studying towards the PhD, degree in the RF & Microwave Research Group at University College Dublin, Ireland.

His research interests include spectrum sensing for cognitive radio, digital predistortion for RF power amplifiers and FPGA hardware implementations.

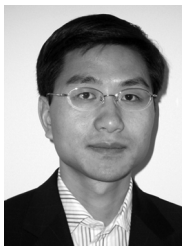

Anding Zhu (S'00-M'04-SM'12) received the B.E. degree in telecommunication engineering from North China Electric Power University, Baoding, China, in 1997, and the M.E. degree in computer applications from Beijing University of Posts and Telecommunications, Beijing, China, in 2000, and the Ph.D. degree in electronic engineering from University College Dublin (UCD), Dublin, Ireland, in 2004.

He is currently a Senior Lecturer with the School of Electrical, Electronic and Communications Engineering, UCD. His research interests include high-frequency nonlinear system modeling and device characterization techniques with a particular emphasis on Volterra-series-based behavioral modeling and linearization for RF PAs. He is also interested in wireless and RF system design, digital signal processing and nonlinear system identification algorithms.